Identification of a Potential Autophagy-Associated Therapeutic Target in Osteosarcoma using Bioinformatic Analyses

Haijun Feng
Second Hospital of Lanzhou University
Liping Wang
Second Hospital of Lanzhou University
Jie Liu
Liaocheng Second People's Hospital
Shengbao Wang (shengbaowang666@gmail.com)
Second Hospital of Lanzhou University https://orcid.org/0000-0002-0001-9890

Research Article

Keywords: autophagy, osteosarcoma, WGCNA, consensus clustering, key gene

Posted Date: December 29th, 2021

DOI: https://doi.org/10.21203/rs.3.rs-1122998/v1

Abstract

Background: Osteosarcoma, primarily resulting from mesenchymal cell differentiation, is the most common primary malignancy of the bone in children and adolescents. Metastases to other sites, such as the lung, often occur in the early stages and progress rapidly. Autophagy functions as a tumor-suppressing mechanism in the early stages of oncogenesis, however, in later stages, autophagy may promote tumor growth, spread, and increase treatment resistance.

Methods: In the present study, we aimed to screen new key autophagy-related biomarkers that may serve as therapeutic targets for osteosarcoma. The expression profile of the GSE42352 dataset, including 103 OS cell lines and 15 MSC lines from Gene Expression Omnibus (GEO), was analyzed to identify the differentially expressed genes.

Results: WGCNA was used to construct the gene co-expression network in osteosarcoma, identify co-expression modules for protein interactions (PPI), and screen the key genes. A total of 757 differentially expressed genes were identified by WGCNA analysis including one key autophagy-related module.

Conclusions: Further, we performed the PPI analysis for module genes and identified a key gene. We also theoretically and functionally validated its expression using the validation dataset GSE14359, and in vitro experiments, respectively.

1 Introduction

Osteosarcoma (OS) is one of the most common malignancies of the bone in children and adolescents under the age of 20, accounting for approximately 5% of childhood tumors; it is associated with a high lethality rate(1–3). Before 1970, amputation was the standard treatment for osteosarcoma, but the five-year overall survival rate was still low, with most patients dying within one year of diagnosis(4). The current 5-year survival rate of patients ranges from 20–60% or 70%(5, 6).

Autophagy was discovered and its mechanism was proposed by Ashford and Porter in 1962(7). Autophagy is a form of cell death where the cells engulf their cytoplasmic proteins or organelles and encapsulate them into vesicles where the contents are eventually degraded(8). It is a dynamic process that promotes organelle and protein turnover. It also generates metabolic precursor molecules through lysosome-dependent degradation of macromolecules, organelles, and other cellular components(9). It is regulated by a variety of autophagy genes, also known as type II programmed cell death. Some studies show that inhibition or activation of autophagy in tumor cells can promote apoptosis and significantly enhance chemotherapeutic efficacy(10). Autophagy promotes tumor growth by mediating levels of cytokines, mTOR, Beclin-1, miRNAs, etc. for the removal of damaged proteins and organelles. For example, during chemotherapy, autophagy is inhibited by miR-22 in osteosarcoma cells(11); Beclin 1 gene plasmid transfection into the MG63 human osteosarcoma cell line showed that with overexpression of Beclin 1, LC3B expression and autophagic activity were enhanced, indicating that Beclin 1 promotes the autophagic process in this tumor cell line(12); the classical autophagic signaling pathway functions

through mTOR, downstream of PI3K/AKT, and is important for controlling translation, cell cycle progression, and negative regulation of autophagy (13). The PI3K/AKT/mTOR pathway has received great attention from researchers in recent years(14, 15)as a major upstream regulator of the autophagic pathway. mTOR-containing protein complexes and other proteins in this pathway are known to be direct or indirect targets of many miRNAs. Thus, a deeper understanding of their underlying mechanisms of action would enhance the treatment strategy for osteosarcoma.

Autophagy can reduce the likelihood of apoptosis by maintaining a range of normal mitochondrial functions such as antioxidant role, anti-DNA damage, and adenosine triphosphate production which promote tumor metastasis(16). It similarly inhibits tumor metastasis by suppressing inflammation and inhibiting macrophage infiltration by parallelly reducing metabolic stress and preventing necrosis-induced death along with apoptosis(17). Thus, autophagy is a complex process involving multiple molecules. It is important to uncover and explore the key factors underlying autophagy for tumor treatment and patient prognosis. In this study, we identified autophagy-associated genes using a bioinformatic approach for osteosarcoma, which can serve as potential biomarkers for the diagnosis and treatment of osteosarcoma.

2 Methodology

2.1 Data sources

GSE42352(18)dataset from Kuijjer ML. et al., containing 103 osteosarcoma- and 15 mesenchymal stem cell samples, and the validation cohort, GSE14359(19)from Fristche-Guenther R. et al., were obtained from the Gene Expression Omnibus (GEO) database. The Human Autophagy Database was used to obtain the detailed and up-to-date expression profiles of 222 autophagy-related genes (ARGs).

2.2 Differential gene expression

The”affy” and the “impute” R packages in R/Bioconductor software were used for GEO data processing, differential gene expression was analyzed with the Limma package (3.40.2) in R. Adjusted P-values were evaluated in GEO to correct for false-positive results. "adjusted P-value < 0.05 and |logFC| ≥ 1" were defined as the cut-off threshold for differential mRNA expression; heat and volcano plots were plotted using the ‘ggplot2’ package in R.

2.3 Autophagy-associated consensus gene clustering

Consensus analysis was performed using the ConsensusClusterPlus package in R (v1.54.0). The maximum number of clusters up to 6 and 100 repetitions were used to extract 80% of the total samples using clusterAlg = "hc", innerLinkage='ward.D2'. The heat map for clustering was analyzed by pheatmap package in R (v1.0.12). The genes with expression variance above 0.1 were included in the heat map; if the number of input target genes was above 1000, the top 25% genes were extracted for display after sorting in descending order of variance. All of these analyses were performed using R v4.0.3.

2.4 Weighted Gene Co-expression Network Analysis (WGCNA)

For the GSE42352 dataset, the WGCNA package in R was used to calculate the Pearson correlation coefficient among the differentially expressed genes. An appropriate soft threshold β was selected to construct the network consistent with the criteria of a scale-free network. A one-step method was used to construct the gene network, transform the adjacency matrix into a topological overlap matrix (TOM), and generate a hierarchical clustering tree of genes. Gene and module significances were calculated. These indicated the significance of genes with clinical information. The module identity (MM) of each gene was calculated and it indicated the importance of the individual gene in the module. Cut-offs were set at |MM|> 0. 8 and |GS|> 0. 2 for gene identification.

2.5 Functional annotation and pathway enrichment analysis

Gene Ontology (GO) and Kyoto Encyclopedia of Genes and Genomes (KEGG) pathway enrichment analyses were performed for all genes in the red module using Database for Annotation, Visualization, and Integrated Discovery (DAVID) (v6.8).

2.6 Protein-protein interaction network (PPI) and hub genes

The STRING database (https://string-db.org/) was used to analyze known and predicted protein-protein interactions. All genes in the red module were analyzed and PPI networks were constructed using STRING. Further, MCODE and Cytohubba in Cytoscape (v3.8.2) software were executed to screen the hub genes in PPI networks.

2.7 Single gene enrichment analysis (GSEA)

The samples were divided into two groups based on the median gene expression as high- and low-expression groups. Gene set enrichment analysis(GSEA) was performed to investigate the functions correlated with different risk groups by GSEA 4.1.0, and the software was downloaded from the website for GSEA (http://www.gseamsigdb.org/gsea/downloads). The association of gene expression with tumors was examined using GSEA. The threshold cut-offs were set at |NES|≥1, FDR<0.25 and P<0.05.

2.8 Cell culture and transfection

The human osteosarcoma cell line, U2OS, was purchased from Yubo Biotechnology Co., Ltd.Shanghai and cultured in DMEM medium (Gibco, USA),containing 10% FBS (Gibco, USA), 100 μg/mL penicillin, and 0.1 mg/mL streptomycin, at 37°C and 5% CO_2. si-CXCR4, an interfering plasmid for CXCR4, and si-NC, the negative control, were designed and synthesized by GenePharma (Shanghai, China). These constructs were transfected into U2OS cells using Lipofectamine 2000 (Invitrogen, Carlsbad, CA, USA) for subsequent experiments.

2.9 Quantitative real-time PCR (qRT-PCR) assay

Total RNA was extracted from cells using TRIzol reagent (Thermo, San Jose, CA, USA). Then the RNA was reversely transcribed by ReverTra Ace® qPCR RT Kit (Toyobo, Osaka, Japan).Real-time PCR reactions were performed using SYBR Green PCR master mix on an ABI7300 real-time PCR machine (Applied Biosystems). The primer sequences were as follow: CXCR4 forward: 5'-GGGCAATGGATTGGTCATCCT-3',reverse:5'-TGCAGCCTGTACTTGTCCG-3'.GAPDH forward:5'-CTGGGCTACACTGAGCACC-3',reverse:5'-AAGTGGTCGTTGAGGGCAATG-3'. The mRNA PCR quantification used the $2^{-\Delta\Delta Ct}$ method against GAPDH for normalization.

2.10 Cell proliferation assay

Cell proliferation was assessed using the Enhanced CCK-8 kit (Beyotime Biotechnology, C0042). Cells were inoculated at a density of 2×10^3 cells/well into 96-well plates for 24h, 48h, 72h, and 96h. 10μL of enhanced CCK-8 solution was added to each well and incubated for 4h at room temperature(20℃-25℃). The absorbance at 450nm was measured using an enzyme marker.

2.11 Trans-well invasion assay

Cells were inoculated at a density of 1×10^5 cells/well into the upper chamber of trans-well pre-wrapped with Matrigel. The lower chamber contained the medium supplemented with 10% FBS The cells were incubated for 24h at room temperature; fixed using paraformaldehyde for 15min; stained with crystal violet for 10min, cells were visualized and counted from six randomly selected fields under a microscope (200 × magnification).

2.12 Cell scratching assay

Cells were inoculated in 24-well plates at a density of 1×10^5 cells/well. After growing to confluence, the cells were scratched using a sterile small gun tip, washed, and incubated for 24 h. The wound healing was observed under the microscope.

2.13 Western blotting

Cells were lysed with cell lysis solution, proteins were extracted, and protein concentrations were determined using the BCA method. After polyacrylamide gel electrophoresis, the proteins were transferred onto the PVDF membrane at a constant current of 300 mA for 90 min. Subsequently, the PVDF membrane was blocked with 5% skimmed milk powder for 2 h. Then p-mTOR (Cell signaling,1:1000), mTOR (Cell signaling,1:1000), p-AKT (Cell signaling,1:1000), and p-AKT (Cell signaling,1:1000), AKT (Cell signaling,1:1000), p-PI3K (Cell signaling,1:1000), PI3K (Cell signaling,1: 1000), Caspase-3 (Cell signaling,1:1000), and GAPDH (Cell signaling,1:1000) primary antibodies were added. After overnight incubation, horseradish peroxidase-labeled secondary antibodies (Cell signaling, diluted 1:3000) were added and the blot was incubated at room temperature for 2 h. In a dark room, the blot was developed on a film using a developer and fixer.

2.14 Statistical analysis

All experiments in this study were repeated at least three times. Statistical analyses were performed using GraphPad Prism 8.0 software. Data were expressed as mean ± standard deviation (x ± s), and a t-test was used for the comparison of two independent data groups. The differences were considered statistically significant at $P<0.05$.

3 Discussion

3.1 DEGs in GSE42352

A total of 103 cancer- and 15-normal cell samples were obtained from the GSE42352 microarray. Heat maps were plotted for the expression of genes in each sample (Figure 1A); a total of 439 up-regulated and 318 down-regulated genes were obtained as presented using the volcano map (Figure 1B). The differentially expressed genes were taken for further functional enrichment analysis, and the top 20 annotated functions and enriched pathways are shown in Figure 1C.

(A: volcano map showing differentially expressed genes; B: heat map showing differentially expressed genes; C: GO enrichment analysis of differentially expressed genes;)

3.2 Consensus clustering based on autophagy-associated genes

To analyze the relationship between the expression of 222 autophagy-related genes and osteosarcoma subtypes, we performed a consensus clustering analysis for 118 samples from GSE42352. On increasing the clustering variable (k) from 2 to 6, we found that at k = 4, the intra-group correlation was the highest and the inter-group correlation was the lowest. This indicated that the 118 samples were well classified into the four clusters (Figure 2A-C). The heat map in Figure 2D shows the gene expression profiles, clinical characteristics, and the ConsensusClusterPlus consistency clustering at k = 4.

(A: CDF curves for k=2-6; B: relative amount of change in area under the CDF curve for consensus clustering at k=2-6; C: 118 samples divided into four groups (k=4) according to the consensus clustering matrix; D: heat map showing clustering results;)

3.3 Identification of gene co-expression modules

To attain the prerequisites of scale-free network distribution, the values of the adjacency matrix weight parameter β needed to be examined. By setting the range of network construction parameters selection, the scale-free distribution topology matrix was calculated. In this study, a soft threshold value of 3 (Figure 3A) was selected to ensure that the scale-free network satisfied the hierarchical clustering, and a total of 36 modules were identified (Figure 3B). The clustering correlation between modules is shown in Figure 3C. The red module was confirmed to be significant by analyzing the correlation of each module with autophagic subtypes and types (Figure 3D-E). Subsequently, KEGG and GO functional enrichment analyses were performed for 1991 genes in the red module, and the significant pathways enriched for the top 20 genes are shown (Figure 3F-G).

(A: soft threshold screening results of constructing scale-free network; B: identification results of TOM-based gene system clustering tree, different colors in the figure represent different multi-gene modules. c: clustering relationship between WGCNA modules and modules; D: heat map of correlation between related traits and module features; E: correlation between red modules and Gene significance; F: KEGG enrichment (analysis of red module genes; G: GO enrichment analysis of red module genes;)

3.4 Construction of PPI network

The DEGs in the red module were analyzed online using the STRING database to obtain the protein interaction network. We visualized the gene information and network construction as shown in Figure 4A. The MCODE plug-in of Cytoscape was used to calculate the characteristics of each node in the network graph. We selected the largest sub-network and visualized it as shown in Figure 4B. MCODE1 functional enrichment is shown in Table 1. Core genes were analyzed with the CytoHubba plug-in; the top 10 genes were identified as core genes using the Closeness algorithm (Figure 4C). These included TLR4, TLR8, ITGAX, ICAM1, CD86, CXCR4, ITGAM, TLR2, TNF, and PTPRC. The overlap between the two analyses showed that CXCR4 was the common core gene (Figure 4D).

(A: PPI plots of genes in the red module; B: MCODE plug-in filtering out the highest-scoring sub-networks; C: Cytohubba plug-in screening the top ten hubba gene networks of the proximity algorithm; D: intersection genes of MCODE1 genes and proximity genes;)

Table 1
MCODE1 functional enrichment

GO		Log10(P)	Log10(q)
R-HSA-418594	G alpha (i) signalling events	-87.37	-83.01
R-HSA-500792	GPCR ligand binding	-79.4	-75.34
R-HSA-372790	Signaling by GPCR	-74.33	-70.45
R-HSA-375276	Peptide ligand-binding receptors	-55.92	-52.34
WP24	Peptide GPCRs	-22.97	-20.21
GO:0072676	lymphocyte migration	-20.25	-17.52
GO:0002407	dendritic cell chemotaxis	-16.72	-14.01
hsa04080	Neuroactive ligand-receptor interaction	-13.73	-11.09
GO:0007200	phospholipase C-activating G protein-coupled receptor signaling pathway	-13.09	-10.47
WP117	GPCRs, Other	-11.57	-9.03
GO:0007188	adenylate cyclase-modulating G protein-coupled receptor signaling pathway	-11.47	-8.93
GO:0051209	release of sequestered calcium ion into cytosol	-10.95	-8.42
GO:1905523	positive regulation of macrophage migration	-9.41	-6.97
R-HSA-416476	G alpha (q) signalling events	-7.23	-4.94
GO:0007218	neuropeptide signaling pathway	-6.08	-3.92
GO:0006968	cellular defense response	-5.73	-3.63
GO:0010759	positive regulation of macrophage chemotaxis	-5.56	-3.47
GO:0042063	gliogenesis	-5.19	-3.14
GO:0007193	adenylate cyclase-inhibiting G protein-coupled receptor signaling pathway	-4.94	-2.92
GO:0051482	positive regulation of cytosolic calcium ion concentration involved in phospholipase C-activating G protein-coupled signaling pathway	-4.67	-2.69

3.5 CXCR4 expression in different datasets

CXCR4 expression was analyzed in different datasets. In the GSE42352 dataset, the expression was significantly high in osteosarcoma cells as compared to the normal cells (Figure 5A). CXCR4 expression differences were statistically significant in all four consensus clustering subtypes of the GSE42352 dataset (Figure 5B); CXCR4 expression was upregulated in the GSE14359 dataset, in the osteosarcoma samples as compared to normal samples (Figure 5C).

(A: CXCR4 expression in the GSE42352 dataset; B: CXCR4 expression in different consensus clustering subgroups; C: CXCR4 expression in the GSE14359 dataset;)

3.6 Functional annotation of single gene CXCR4

The five KEGG and HALLMARK pathways that were most significantly associated with high CXCR4 expression are shown in Figure 6. Among these, CXCR4 was mainly enriched in arachidonic acid metabolism, natural killer cell-mediated cytotoxicity, systemic lupus erythematosus, toll-like receptor signaling pathway, and B-cell receptor signaling pathway (Figure 6A). Additionally, CXCR4 high expression was positively associated with complement pathway, apoptosis, coagulation, IL-6/JAK/STAT3 signaling system, and heme metabolism (Figure 6B).

(A: KEGG enrichment analysis; B: HALLMARK enrichment analysis)

3.7 In vitro CXCR4 assay

In the present study, we evaluated CXCR4 expression in cell lines by quantitative real-time PCR,the results showed that CXCR4 siRNA led to a marked reduction of CXCR4 mRNA expression level(Figure 7A). CCK-8 assay was used to detect the effect of CXCR4 on cell proliferation. The results indicated that the proliferation of U2OS cells transfected with si-CXCR4 was significantly inhibited (Figure 7B). Trans-well invasion assay and cell scratch assay were used to analyze the effect of CXCR4 on cell invasion and migration. The results showed that the invasion ability of U2OS cells transfected with si-CXCR4 was significantly reduced and the scratch spacing was significantly increased as compared to the untransfected U2OS cells and si-NC group. Thus, the invasion and migration of the cells were diminished (Figure 7C-7D). We used western blotting to examine the expression of autophagic pathway-related proteins in U2OS cells. si-CXCR4 transfection significantly decreased the levels of PI3K, AKT, and mTOR phosphorylation and elevated the levels of Caspase-3 protein expression in U2OS cells (Figure 7E). These results suggested that CXCR4 silencing induced autophagic cell death through the inhibition of the PI3K/AKT/mTOR signaling pathway but did not inhibit the growth in osteosarcoma.

(A: qPCR assay; B: CCK-8 assay; C: Transwell invasion assay; D: scratch assay; E: Western blot; **is compared with U2OS or si-NC, $P<0.01$;)

4 Conclusion

In recent years, the number of studies based on public databases such as GEO and TARGET has increased. These are useful to mine potential biomarkers for osteosarcoma. For example, Dai et al.

(20)screened candidate genes to predict the chemotherapy resistance response of osteosarcoma by miRNA-mRNA interaction network. Jiang et al. (21) identified autophagy and immune-related gene markers TRIM68, PIKFYVE, and DYNLL2, which could predict the prognosis of osteosarcoma. In the present study, using the GSE42352 dataset and by differential WGCNA analysis, we screened autophagy-related modular genes and construct a PPI network. A key gene, CXCR4, was identified by MCODE and Closeness algorithms. 222 autophagy-related genes were obtained from the online database. We performed concordance analysis for samples in GSE42352, and four subgroups were obtained; CXCR4 was identified in all four subgroups. Using the validation dataset GSE14359, we showed that CXCR4 was indeed highly expressed in osteosarcoma as compared to normal samples. Niu et al.(22) have also identified CXCR4 as a possible therapeutic agent to inhibit the progression of osteosarcoma by bioinformatic analysis.

Chemokine receptor-4 (CXCR4) is a specific receptor for chemokine stromal cell-derived factor-1 (CXCL12) (23). There is increasing evidence that CXCR4 plays a crucial role in osteosarcoma progression and metastasis(24, 25). In addition, CXCR4 is associated with poor survival in patients with osteosarcoma and is considered to be an important clinical prognostic indicator(26). In the present study, the module selected for WGCNA analysis showed the highest significant correlation with autophagy. Autophagy, a highly evolutionarily conserved cellular homeostatic dynamic recycling system, is used for cytoplasmic recycling, degradation, and reuse(27). Autophagy selectively degrades long-lived proteins, removes dysfunctional organelles under basal conditions, and promotes cell survival(28). It has been recognized as a cytoprotective process that promotes chemoresistance in osteosarcoma. Several studies have focused on autophagy inhibition in osteosarcoma chemo-sensitization(29). Coly et al.(30) found that, in HEK293 and U87 cells, activation of CXCR4 leads to a decrease in the number of autophagosomes, suggesting that CXCR4 exerts its anti-autophagic effect by regulating calcium-activating enzymes and preventing pre-autophagosomal vesicle formation. In the present study, our in vitro assays also showed that CXCR4 could affect the progression of osteosarcoma by regulating the PI3K-Akt-mTOR signaling pathway. The main regulator of autophagy is mTORC1; mTORC2 also contributes to the autophagic control through AKT pathway regulation(31). Under normal conditions, mTORC1 directly inactivates the ULK1/2 protein complexes. These complexes are critical and essential regulators of cellular pathways that control the initiation of gene translation and ribosome biogenesis and exhibit important monitoring roles for cellular metabolism, lipolysis, and autophagy (32, 33). In general, there is a negative interaction between autophagy and apoptosis, as autophagy prevents apoptosis induction and apoptosis-associated caspase activation inhibits the autophagic process. Some studies also show that the negative correlation between CXCR4 and autophagy is dependent on PI3K/AKT/mTOR signaling pathway (34).

In the present study, by single gene enrichment analysis, we showed that CXCR4 is mainly enriched in arachidonic acid metabolism, natural killer cell-mediated cytotoxicity, and IL-6/JAK/STAT3 signaling pathway in osteosarcoma. Previous studies(35) have shown that CXCR4 is itself involved in NK cell-mediated cytotoxicity in chronic granulocytic leukemia. IL-6/JAK/STAT3 is a stress-related inflammatory signaling pathway, with rapid response. Dysregulated cytokine signaling contributes to cancer development (36). In addition, the STAT family of transcription factors can be regulated by other kinases,

such as mTOR, MAPK which phosphorylate Ser727 of STAT3 for sustained activation (37). STAT3 is potentially pro-oncogenic (a proto-oncogene) and is consistently expressed across several cancers. In the pathogenesis of atherosclerosis, CXCR4 is involved in chronic inflammation of the arterial wall and is characterized by a chemokine-mediated inward flow of leukocytes(38). Chronic inflammation and local infiltration of CXCR4-expressing immune cells can promote esophageal carcinogenesis(39). Activating downstream cascades involving JAK/STAT, PI3K/Akt, MAPK, JNK pathway considered important targets for development of new therapeutic strategies, and the activation can be triggered by the binding between CXCR4 and its ligand CXCL12. These critical points control stemness, chemotaxis and cell survival, proliferation, migration(40). CXCL12(41, 42) is a homeostatic chemokine produced by mesenchymal stem cells,which binds to chemokine receptors to regulate hematopoietic stem cell (HSC) transport and secondary lymphoid tissue structure. CXCR4 overexpression has been found in many tumors(43). There are evidences that CXCR4/CXCL12 axis activates multiple downstream pathways and plays an important role in tumor progression(41, 44).Besides, previous study have found that the overwhelming majority of metastases from osteosarcoma are to the lung, a site that expresses high levels of the ligand CXCL12(45).

Taken together, our results systematically demonstrated high CXCR4 expression in osteosarcoma. We speculated that it could induce autophagic cell death by regulating the PI3K/AKT/mTOR signaling pathway. Indeed, functional enrichment analysis showed that CXCR4 in inflammatory, immune-related contexts could provide new strategies for gene-targeted therapy for osteosarcoma.

Declarations

Ethics approval and consent to participate: none

Consent for publication: none

Availability of data and materials: none

Competing interests: none

Funding: none

Authors' contributions: we contributed equally for this work

Acknowledgements: none

References

1. de Azevedo JWV, Fernandes TAAdM, Fernandes JV, de Azevedo JCV, Lanza DCF, Bezerra CM, et al. Biology and pathogenesis of human osteosarcoma. Oncology letters. 2020;19(2):1099–116.
2. Lindsey BA, Markel JE, Kleinerman ES. Osteosarcoma overview. Rheumatology therapy. 2017;4(1):25–43.

3. Wu B, Yang W, Fu Z, Xie H, Guo Z, Liu D, et al. Selected using bioinformatics and molecular docking analyses, PHA-793887 is effective against osteosarcoma. Aging. 2021;13(12):16425.
4. Rosen G, Tan C, Sanmaneechai A, Beattie EJ Jr, Marcove R, Murphy ML. The rationale for multiple drug chemotherapy in the treatment of osteogenic sarcoma. Cancer. 1975;35(S3):936–45.
5. Rosen G, Huvos AG, Mosende C, Beattie EJ Jr, Exelby PR, Capparos B, et al. Chemotherapy and thoractomy for metastatic osteogenic sarcoma. A model for adjuvant chemotherapy and the rationale for the timing of thoracic surgery. Cancer. 1978;41(3):841–9.
6. Whelan J, Seddon B, Perisoglou M. Management of osteosarcoma. Curr Treat Options Oncol. 2006;7(6):444–55.
7. Ashford TP, Porter KR. Cytoplasmic components in hepatic cell lysosomes. J Cell Biol. 1962;12(1):198–202.
8. Levine B, Kroemer G. Autophagy in the pathogenesis of disease. Cell. 2008;132(1):27–42.
9. Huang J, Liu K, Yu Y, Xie M, Kang R, Vernon PJ, et al. Targeting HMGB1-mediated autophagy as a novel therapeutic strategy for osteosarcoma. Autophagy. 2012;8(2):275–7.
10. Wang F, Cao M, Fan M, Wu H, Huang W, Zhang Y, et al. AMPK-mTOR-ULK1 axis activation-dependent autophagy promotes hydroxycamptothecin-induced apoptosis in human bladder cancer cells. Journal of cellular physiology. 2020;235(5):4302–15.
11. Li X, Wang S, Chen Y, Liu G, Yang X. miR-22 targets the 3' UTR of HMGB1 and inhibits the HMGB1-associated autophagy in osteosarcoma cells during chemotherapy. Tumor Biology. 2014;35(6):6021–8.
12. Tao H, Chen F, Liu H, Hu Y, Wang Y, Li H. Wnt/β-catenin signaling pathway activation reverses gemcitabine resistance by attenuating Beclin1-mediated autophagy in the MG63 human osteosarcoma cell line. Mol Med Rep. 2017;16(2):1701–6.
13. Jung CH, Ro S-H, Cao J, Otto NM, Kim D-H. mTOR regulation of autophagy. FEBS Lett. 2010;584(7):1287–95.
14. Zhou J, Jiang Yy, Chen H, Wu Y, Zhang L. Tanshinone I attenuates the malignant biological properties of ovarian cancer by inducing apoptosis and autophagy via the inactivation of PI3K/AKT/mTOR pathway. Cell proliferation. 2020;53(2):e12739.
15. Liu H, Gong X, Yang K. Overexpression of the clock gene Per2 suppresses oral squamous cell carcinoma progression by activating autophagy via the PI3K/AKT/mTOR pathway. J Cancer. 2020;11(12):3655.
16. El Hout M, Cosialls E, Mehrpour M, Hamaï A. Crosstalk between autophagy and metabolic regulation of cancer stem cells. Mol Cancer. 2020;19(1):1–17.
17. Fan X, Zhang H, Cheng Y, Jiang X, Zhu J, Jin T. Double roles of macrophages in human neuroimmune diseases and their animal models. Mediators of inflammation. 2016;2016.
18. Kuijjer ML, Peterse EF, van den Akker BE, Briaire-de Bruijn IH, Serra M, Meza-Zepeda LA, et al. IR/IGF1R signaling as potential target for treatment of high-grade osteosarcoma. BMC Cancer.

2013;13(1):1–9.
19. Noske A, Ungethüm U, Kuban R-J, Schlag P, Tunn P-U, Karle J, et al. De novo expression of EphA2 in osteosarcoma modulates activation of the mitogenic signaling pathway. 2010.
20. Dai P, He Y, Luo G, Deng J, Jiang N, Fang T, et al. Screening candidate microRNA-mRNA network for predicting the response to chemoresistance in osteosarcoma by bioinformatics analysis. Journal of cellular biochemistry. 2019;120(10):16798–810.
21. Jiang J, Liu D, Xu G, Liang T, Yu C, Liao S, et al. TRIM68, PIKFYVE, and DYNLL2: The novel autophagy-and immunity-associated gene biomarkers for osteosarcoma prognosis. Front Oncol. 2021;11:1238.
22. Niu J, Yan T, Guo W, Wang W, Zhao Z, Ren T, et al. Identification of potential therapeutic targets and immune cell infiltration characteristics in osteosarcoma using bioinformatics strategy. Front Oncol. 2020;10:1628.
23. Liao Y-X, Zhou C-H, Zeng H, Zuo D-Q, Wang ZY, Yin F, et al. The role of the CXCL12-CXCR4/CXCR7 axis in the progression and metastasis of bone sarcomas. Int J Mol Med. 2013;32(6):1239–46.
24. Zhu Y, Tang L, Zhao S, Sun B, Cheng L, Tang Y, et al. CXCR 4-mediated osteosarcoma growth and pulmonary metastasis is suppressed by Micro RNA-613. Cancer Sci. 2018;109(8):2412–22.
25. Pollino S, Palmerini E, Dozza B, Bientinesi E, Piccinni-Leopardi M, Lucarelli E, et al. CXCR4 in human osteosarcoma malignant progression. The response of osteosarcoma cell lines to the fully human CXCR4 antibody MDX1338. Journal of bone oncology. 2019;17:100239.
26. Li Y-J, Dai Y-L, Zhang W-B, Li S-J, Tu C-Q. Clinicopathological and prognostic significance of chemokine receptor CXCR4 in patients with bone and soft tissue sarcoma: a meta-analysis. Clinical experimental medicine. 2017;17(1):59–69.
27. Liu B, Lu Y, Zhang T, Yu X, Wang Q, Chi Y, et al. CMTM7 as a novel molecule of ATG14L-Beclin1-VPS34 complex enhances autophagy by Rab5 to regulate tumorigenicity. Cell Communication Signaling. 2021;19(1):1–16.
28. Lin L, Baehrecke EH. Autophagy, cell death, and cancer. Molecular cellular oncology. 2015;2(3):e985913.
29. Kim M, Jung J-Y, Choi S, Lee H, Morales LD, Koh J-T, et al. GFRA1 promotes cisplatin-induced chemoresistance in osteosarcoma by inducing autophagy. Autophagy. 2017;13(1):149–68.
30. Coly P-M, Perzo N, Le Joncour V, Lecointre C, Schouft M-T, Desrues L, et al. Chemotactic G protein-coupled receptors control cell migration by repressing autophagosome biogenesis. Autophagy. 2016;12(12):2344–62.
31. Kakiuchi Y, Yurube T, Kakutani K, Takada T, Ito M, Takeoka Y, et al. Pharmacological inhibition of mTORC1 but not mTORC2 protects against human disc cellular apoptosis, senescence, and extracellular matrix catabolism through Akt and autophagy induction. Osteoarthritis cartilage. 2019;27(6):965–76.
32. Laplante M, Sabatini DM. mTOR signaling in growth control and disease. Cell. 2012;149(2):274–93.

33. Zoncu R, Efeyan A, Sabatini DM. mTOR: from growth signal integration to cancer, diabetes and ageing. Nature reviews Molecular cell biology. 2011;12(1):21–35.
34. Liao Y-X, Lv J-Y, Zhou Z-F, Xu T-Y, Yang D, Gao Q-M, et al. CXCR4 blockade sensitizes osteosarcoma to doxorubicin by inducing autophagic cell death via PI3K–Akt–mTOR pathway inhibition. Int J Oncol. 2021;59(1):1–11.
35. Herrmann AB, Müller ML, Orth MF, Müller JP, Zernecke A, Hochhaus A, et al. Knockout of LASP1 in CXCR4 expressing CML cells promotes cell persistence, proliferation and TKI resistance. J Cell Mol Med. 2020;24(5):2942–55.
36. Johnson DE, O'Keefe RA, Grandis JR. Targeting the IL-6/JAK/STAT3 signalling axis in cancer. Nature reviews Clinical oncology. 2018;15(4):234–48.
37. Ni Y, Wu S, Wang X, Zhu G, Chen X, Ding Y, et al. Cucurbitacin I induces pro-death autophagy in A549 cells via the ERK-mTOR-STAT3 signaling pathway. Journal of cellular biochemistry. 2018;119(7):6104–12.
38. Galkina E, Ley K. Immune and inflammatory mechanisms of atherosclerosis. Annual review of immunology. 2009;27.
39. Fang H-Y, Münch NS, Schottelius M, Ingermann J, Liu H, Schauer M, et al. CXCR4 is a potential target for diagnostic PET/CT imaging in Barrett's dysplasia and esophageal adenocarcinoma. Clin Cancer Res. 2018;24(5):1048–61.
40. Cojoc M, Peitzsch C, Trautmann F, Polishchuk L, Telegeev GD, Dubrovska A. Emerging targets in cancer management: role of the CXCL12/CXCR4 axis. OncoTargets therapy. 2013;6:1347.
41. Teicher BA, Fricker SP. CXCL12 (SDF-1)/CXCR4 pathway in cancer. Clinical cancer research. 2010;16(11):2927–31.
42. Domanska UM, Kruizinga RC, Nagengast WB, Timmer-Bosscha H, Huls G, de Vries EG, et al. A review on CXCR4/CXCL12 axis in oncology: no place to hide. European journal of cancer. 2013;49(1):219–30.
43. Liang J-X, Gao W, Liang Y, Zhou X-M. Chemokine receptor CXCR4 expression and lung cancer prognosis: a meta-analysis. Int J Clin Exp Med. 2015;8(4):5163.
44. Kim RH, Li BD, Chu QD. The role of chemokine receptor CXCR4 in the biologic behavior of human soft tissue sarcoma. Sarcoma. 2010;2011.
45. Kim SY, Lee CH, Midura BV, Yeung C, Mendoza A, Hong SH, et al. Inhibition of the CXCR4/CXCL12 chemokine pathway reduces the development of murine pulmonary metastases. Clin Exp Metastasis. 2008;25(3):201–11.

Figures

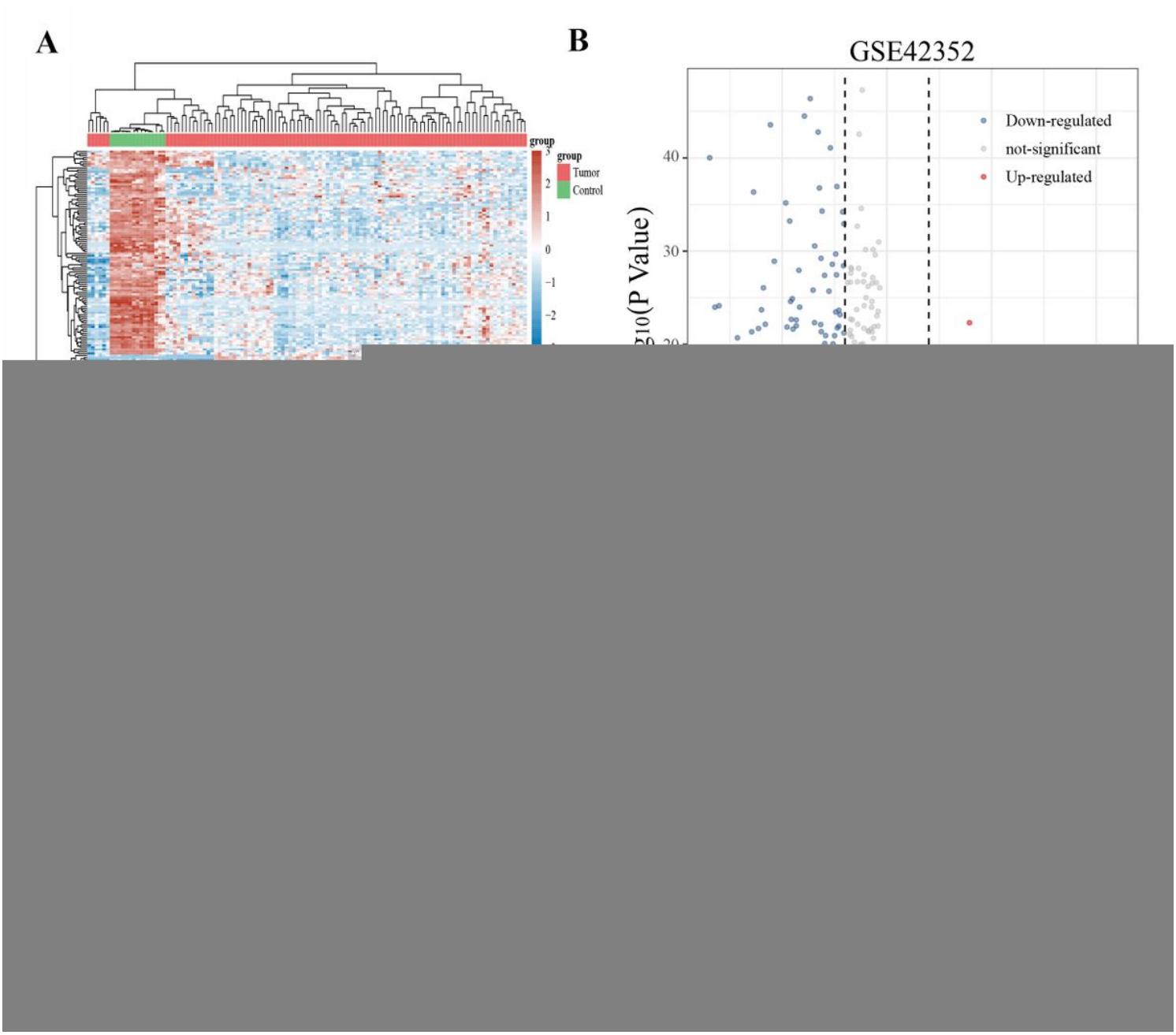

Figure 1

Differentially expressed genes in GSE42352

(A: volcano map showing differentially expressed genes; B: heat map showing differentially expressed genes; C: GO enrichment analysis of differentially expressed genes;)

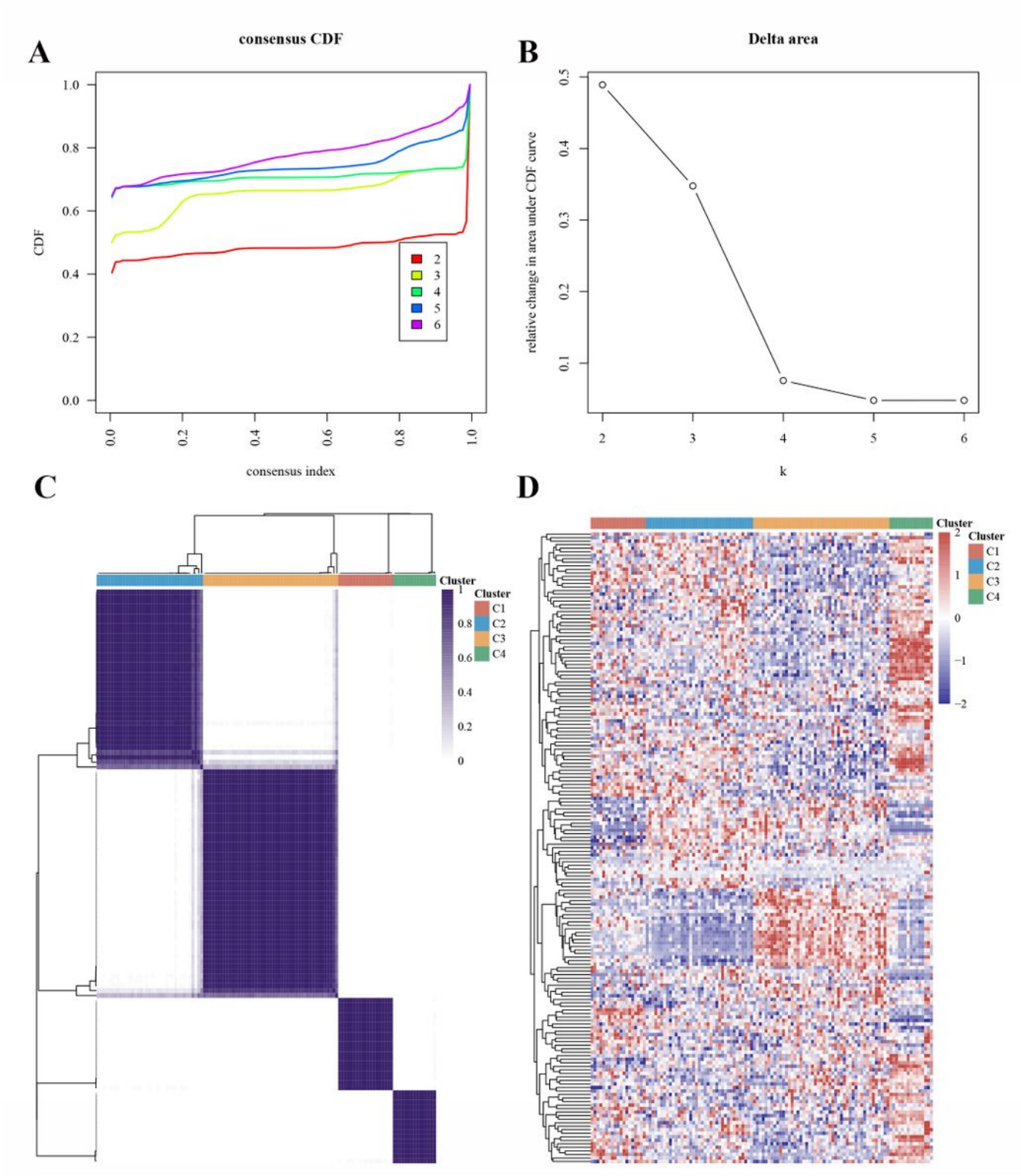

Figure 2

Consensus clustering of tumors based on autophagy-related genes

(A: CDF curves for k=2-6; B: relative amount of change in area under the CDF curve for consensus clustering at k=2-6; C: 118 samples divided into four groups (k=4) according to the consensus clustering matrix; D: heat map showing clustering results;)

Figure 3

Identification of gene co-expression modules

(A: soft threshold screening results of constructing scale-free network; B: identification results of TOM-based gene system clustering tree, different colors in the figure represent different multi-gene modules. c: clustering relationship between WGCNA modules and modules; D: heat map of correlation between related traits and module features; E: correlation between red modules and Gene significance; F: KEGG enrichment (analysis of red module genes; G: GO enrichment analysis of red module genes;)

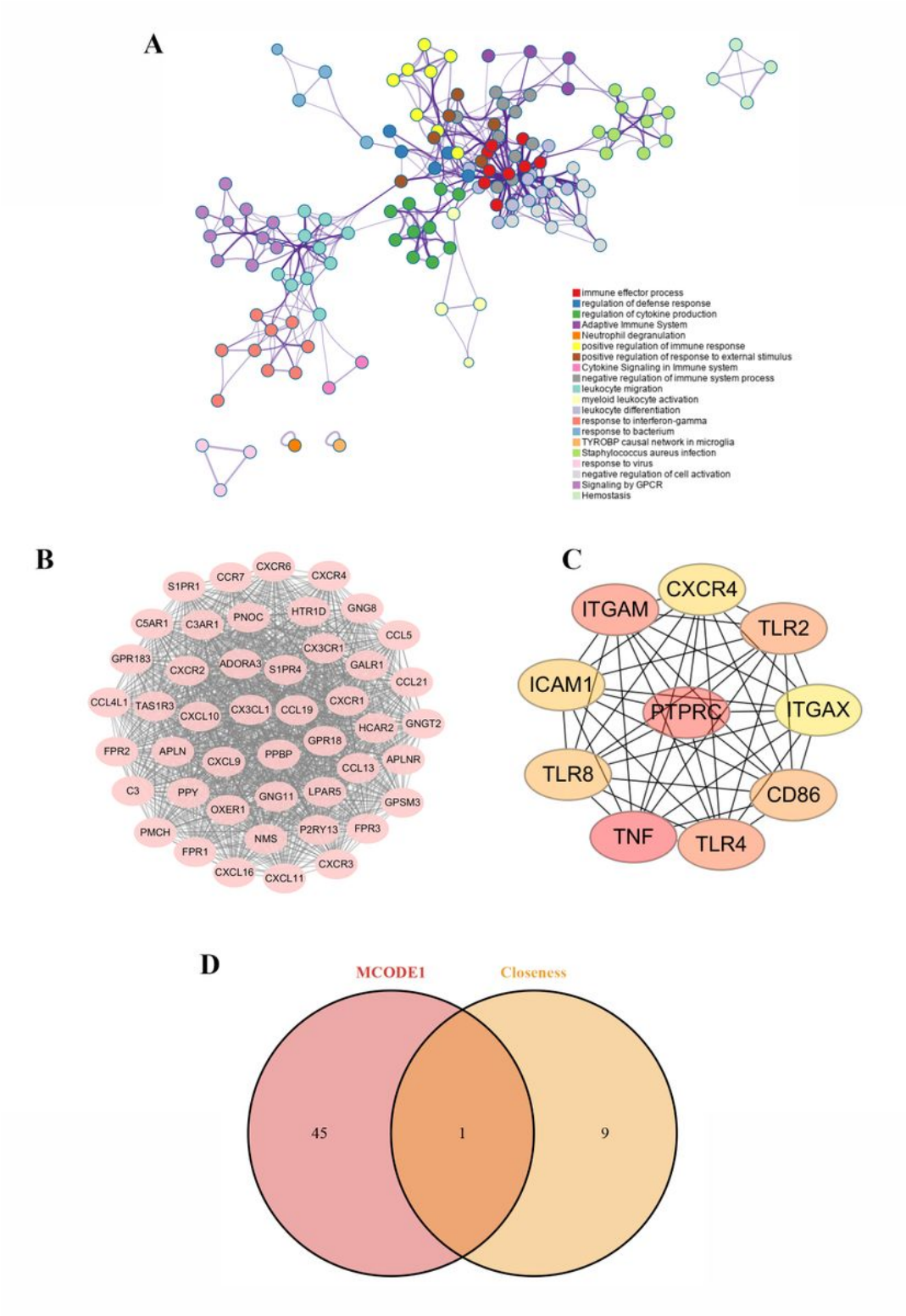

Figure 4

PPI protein network analysis and core gene identification

(A: PPI plots of genes in the red module; B: MCODE plug-in filtering out the highest-scoring sub-networks; C: Cytohubba plug-in screening the top ten hubba gene networks of the proximity algorithm; D: intersection genes of MCODE1 genes and proximity genes;)

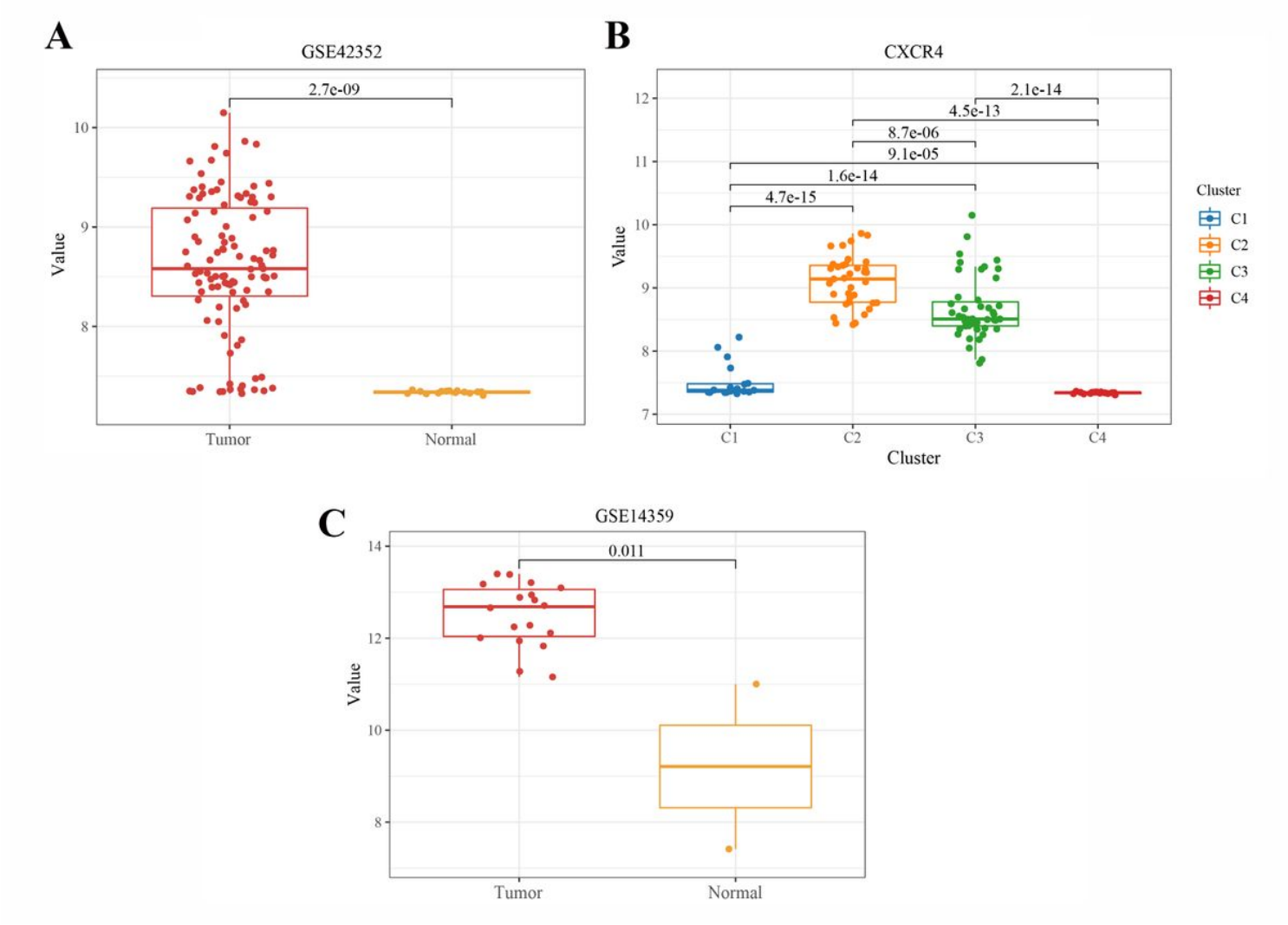

Figure 5

Expression of CXCR4 in different datasets

(A: CXCR4 expression in the GSE42352 dataset; B: CXCR4 expression in different consensus clustering subgroups; C: CXCR4 expression in the GSE14359 dataset;)

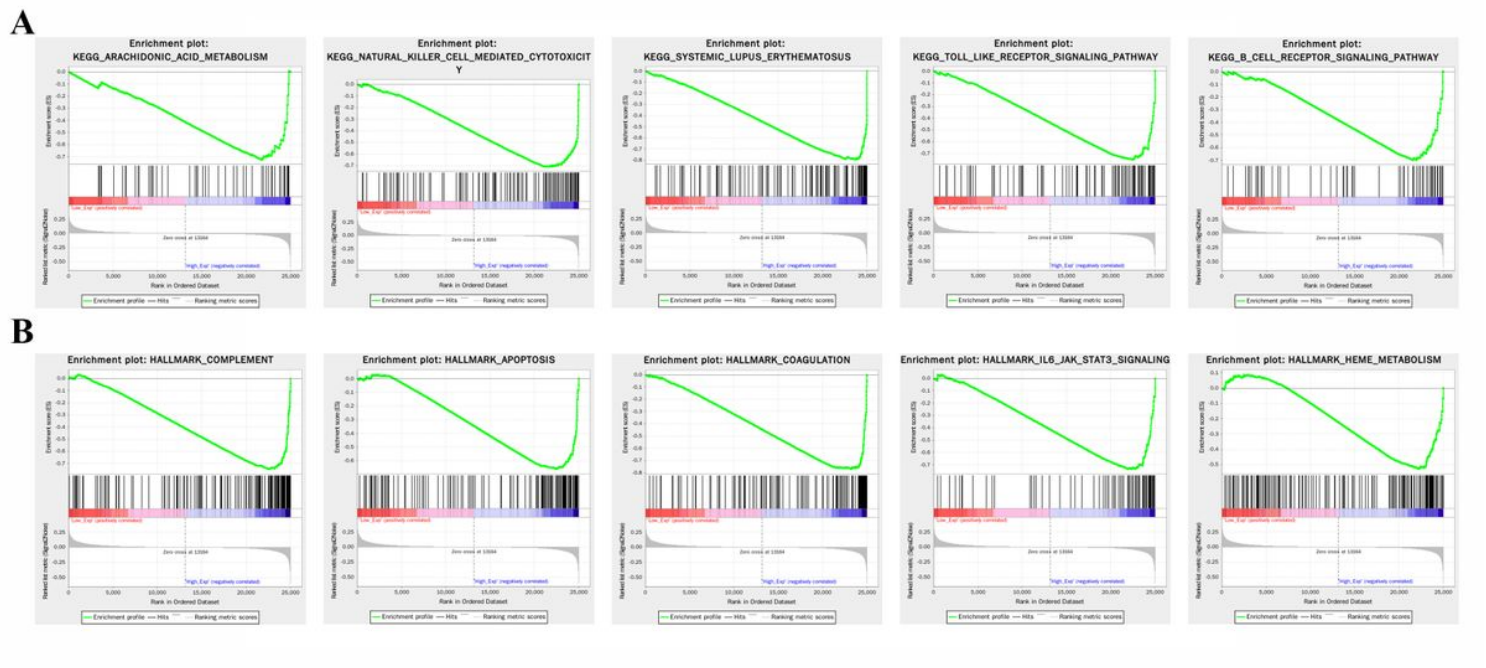

Figure 6

Single gene enrichment analysis of CXCR4

(A: KEGG enrichment analysis; B: HALLMARK enrichment analysis)

Figure 7

CXCR4 in vitro assay

(A: qPCR assay; B: CCK-8 assay; C: Transwell invasion assay; D: scratch assay; E: Western blot; **is compared with U2OS or si-NC, P<0.01;)